Acoustical Methods and Experiments for Studying Rotorcraft Fuselage Scattering

Jianping Yin
Research Scientist
DLR
Braunschweig, Germany

Karl-Stéphane Rossignol
Research Scientist
DLR
Braunschweig, Germany

Mattia Barbarino
Research Scientist
CIRA
Capua, Italy

Davide Bianco
Research Scientist
CIRA
Capua, Italy

Claudio Testa
Research Scientist
CNR-INSEAN
Rome, Italy

Harry Brouwer
Research Scientist
NLR
Amsterdam, Netherlands

Stevie Ray Janssen
Research Scientist
NLR
Amsterdam, Netherlands

Gabriel Reboul
Research Scientist
ONERA
Paris, France

Luigi Vigevano
Associate Professor
Politecnico di Milano
Milano, Italy

Giovanni Bernardini
Professor
Roma TRE University
Rome, Italy

Massimo Gennaretti
Professor
Roma TRE University
Rome, Italy

Jacopo Serafini
Professor
Roma TRE University
Rome, Italy

Caterina Poggi
PhD Student
Roma TRE University
Rome, Italy

ABSTRACT

This paper deals the activities conducted in the GARTEUR Action Group HC/AG-24 to address noise scattering of helicopter rotors in presence of the fuselage. The focus of the Action Group is on the development and validation of numerical prediction methods and establishing an experimental data base for numerical validations. The numerical methods applied by most partners solve the Helmholtz equation using a Boundary Element Method for addressing the discretized Green's function integral formulation of the solution. The test activities are conducted in the DLR Acoustic Wind Tunnel in Braunschweig (AWB), including acoustic scattering tests by spheres and a generic helicopter model. In the current paper, the results from the numerical simulations, the wind tunnel tests as well as numerical and test comparisons are addressed. The test configurations include the spheres with sting support and a finite NACA0012 wing (thanks to share data with a NATO STO group). The acoustic predictions of the scattering by spheres will be compared with the analytic solution to address the influence of the sphere support systems at different wind speeds. The acoustic predictions of the scattering by NACA0012 wing will be analyzed and compared to available test results for different source locations and frequencies.

NOTATION

D Diameter of the sphere
f Frequency
p_{tot} Total acoustic pressure perturbation
p_i Incident acoustic pressure perturbation
p_s Scattered acoustic pressure perturbation
γ_T Shielding factor $\gamma_T = p_{tot}/p_i$ or $\langle p_{tot}\rangle / \langle p_i \rangle$ for numerical or test results, respectively

r Observer position
r_0 Magnitude of the vector from source to observer
r_s Source position
R Radius of the sphere
V Flow speed
ψ Azimuth angle
θ Polar angle
AG Action Group
AWB Acoustic Wind tunnel in Braunschweig

BEM	Boundary Element Method
GARTEUR	Group for Aeronautic Research and Technology in Europe
HC	Helicopter
PPW	Point Per Wave length
SPARC	Source-imPulsionnelle AeRoaCoustique
STO	Science and Technology Organization

1. INTRODUCTION

Helicopter noise reduction is a long term objective of the helicopter industry in view of extending the market to new civil applications, as well as getting prepared to comply with new and increasingly stringent noise regulation. Both the main and the tail rotors (including Fenestron) of a helicopter are major sources of noise and contribute significantly to its ground noise footprint. The research efforts in the past were mainly concentrated on the helicopter rotor noise generation and reduction. Even though the scattering of noise generated by helicopter rotors has been recognized as having a significant influence on the noise spectra and directivity generated by isolated rotating blades, there has not been an extensive research effort towards the comprehension of the phenomenon. This is particularly important when dealing with the tail rotor noise, for which the wavelength of the harmonics is comparable or smaller than the characteristic dimension of the fuselage. In order to boost research activities on noise propagation in presence of the fuselage a specific Action Group (AG24) [1][2][3] has been constituted in the Helicopter Group of Responsables framework of the Group for Aeronautical Research and Technology in EURope (GARTEUR). The focus has been put on the development and validation of numerical prediction methods, addressed within the WP1 of the AG. The experimental activities are carried out in the second WP of the AG. The objectives of this AG are (1) to expand the limits of current noise prediction tools, so that the shielding effects and controlled surface impedance can be exploited for the development of new vehicles thus reducing the environmental impact of helicopters and increasing public acceptance and (2) to generate a unique noise scattering database through wind tunnel test using generic configurations, such as spheres of different materials (wood or aluminium), wings and a GARTEUR helicopter model composed of an ellipsoid fuselage, cylinder tail boom and a simple empennage.

In the current paper, the results from the numerical simulations, wind tunnel tests as well as numerical and test comparisons are addressed. The test configurations include the spheres with sting support and a finite NACA0012 wing (thanks to share data with a NATO STO group). One purpose of choosing spheres in the test is to verify the accuracy of the complete test system, such as support systems and noise sources, microphones as well as the reliability of the test results. By comparing with analytic solutions, the influence of the sphere support systems and different wind speeds can be addressed.

This paper is organized as follows: the methodologies applied in the numerical simulations by GARTEUR partners will be first described; the introduction of the experimental approach used in the acoustic scattering test, including noise sources, wind tunnel models, acoustic instrumentation and data reduction will then be presented; the acoustic scattering predictions from the sphere and from the NACA0012 wing will be analyzed and compared with available test results for different source positions and frequencies. In addition a comparison with analytic or numerical results is also presented to assess the accuracy of the test system.

2. DESCRIPTION OF METHODOLOGIES APPLIED IN NUMERICAL SIMULATIONS BY THE PARTNERS

In this section, a brief description of the scattering formulations used by the AG partners is presented. Figure 1 summarizes the computational methodology used when a BEM code is employed for a point source scattering problem.
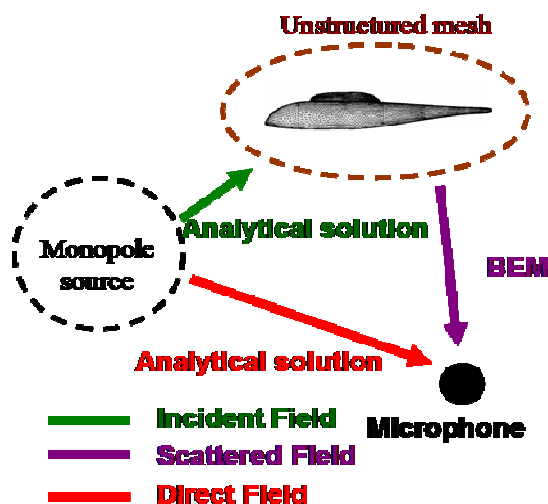

Figure 1. Computational methodology using BEM

As shown in Figure 1, the incident field from the source is indicated by the green arrow and can be obtained by either analytical solution or numerical one. For a conventional BEM code, the required inputs are the incident pressure field and the normal

pressure gradient on the scattering surface and BEM code then provides scattered radiation indicated by the purple arrow. Both the direct field (the red arrow) and the scatted field (the purple arrow) add in the microphone position to construct an overall sound pressure. The BEM codes used by all partners are the frequency domain codes. The unstructured mesh is used by all partners, except the University of RomaTRE and CNR-INSEAN.

The CIRA BEM code, OptydB-BEM [4][5], has the possibility to include the effect of the fluid velocity, solving the convected Helmholtz equation formulated either in pressure (Lighthill's analogy) or in terms of the velocity scalar potential (Howe/Pierce analogy). The uniform mean flow effect is treated by means of the convected free-field Green functions. The integral equations are treated using the collocation approach and the Combined Helmholtz Integral Equation Formulation (CHIEF) for removing the spurious frequencies. The discrete set of equations associated then with the boundary problem is solved with an iterative approach. The code can manage unstructured grids with triangular and quadrilateral elements and different types of boundary conditions. At last a black-box directional, Fast Multipole Method (FMM) is implemented for dealing with large scattering problems.

DLR is using the Fast Multipole Boundary Element Method (FMBEM) code [6] which solves the exterior Helmholtz problem for the scattered pressure field. It is a BEM method which employs the Fast Multipole Method (FMM) for triangulated surfaces. FMBEM uses an iterative solver from PETSc library as well as OpenMP/MPI parallelization for the fast evaluation of matrix-vector products so that no storage of the matrix is required. In addition, the Burton-Miller approach [11] is used to guarantee the uniqueness of the solution. Based on the assumption of low Mach number potential flow, a Taylor transformation of the convected wave equation in the Helmholtz equation is used to take into account the mean flow effect [13]. Similar to ONERA method, a post-processing is used following [13] to deal with potential flow effect.

NLR uses its in-house finite-volume CFD/CAA code ENFLOW [7]. It solves the linearized Euler equations for a given non-uniform steady flow-field on a block-structured, boundary-conforming grid. The code utilizes a 4th order accurate low dispersion & dissipation scheme to be able to propagate acoustic disturbances over large distances. Generation of spurious waves is avoided by implementation of 6th order artificial diffusion, and the use of non-reflecting boundaries. The code uses an explicit 4th order Runge-Kutta scheme to advance the solution in time.

ONERA is using two different acoustic scattering codes. The goal is to identify the limitation of the first using the later as a reference. The simplest method is based on the Kirchhoff integral with the assumption of a locally flat surface with single reflections. This methodology is implemented in ONERA FW-H code named KIM [8]. Compare to BEM, this approach has the advantage to be fast and to be implemented in the time-domain which could be interesting when dealing with multi-frequency application and impulsive phenomenon such as BVI for example. The second approach used at ONERA is the BEM code named BEMUSE[9]. The Onera's in-house BEMUSE code solves this system using either a Brakhage Werner [10] or Burton-Miller integral formulations[11]. Sommerfeld radiation condition is applied at infinity and the scattering surface defines the boundary conditions which can be for instance Neumann, Dirichlet or Robin ones. These elements are coupled with an algebraic approach of the kernel approximation (inverse matrix) based on the Adaptive Cross Approximation (ACA) method. The implemented method is following the works of Grasedyck [12] on asymptotically smooth kernel operators. It computes a low–rank approximation of appropriate matrix blocks, independent on the kernel operator. Even if convection effects are not taken into account in BEMUSE, a post-processing is used following [13] to deal with potential flow effect. The following equation is used to compute the total acoustic pressure ($p(x,t)$) thanks to the solution of the Helmholtz equation (Φ_h) and the mean flow velocity potential (φ):

$$
\begin{aligned}
p(x,t) &= -\rho(-i\omega\Phi_h + \nabla\varphi.\nabla\Phi_h) \\
&\quad .\exp\left\{i\omega[\varphi(x_o) - \varphi(x)]/a_o^2\right\}\exp(-i\omega t)
\end{aligned}
$$

where ρ is the free-stream mean density and x and x_o are the field and source location, respectively.

For validation purpose ONERA has also performed a CAA computation on the NACA0012 test case. sAbrinA-v0 is a structured grid, time-accurate code that solves either the full or the linear Euler equations, in a conservative and perturbed form (with a splitting of the complete variables into a "frozen" mean flow and a "fluctuating" perturbation). The solver employs high-order, finite difference operators, involving a 3rd-order, multi-stage, Runge-Kutta time-marching scheme. The code deals with multi-block structured grids with one-to-one interfaces, and is fully parallelized using the Message Passing Interface (MPI) standard. More detailed information about the sAbrinA-v0 solver and its underlying methodology can be found in

reference [14]. In this application a newly developed Immersed Boundary Condition has been applied [15].

Differently, the University of RomaTRE and CNR-INSEAN have developed a non standard tool, in the frequency domain, based on the boundary integral solution of the Ffowcs-Williams and Hawkings Equation for the scattering analysis of moving/elastic bodies [16]. Beside this pressure-based approach, the Helmholtz equation for the velocity potential is also proposed to compute the scattered pressure field [16]. Both formulations use the CHIEF method to remove spurious frequencies effects (if present). Recently, the potential-based formulation has been extended to include nonlinear effects due to the steady-state aerodynamic mean flow: a first-order formulation based on the linearization of nonlinearity about the steady-state aerodynamic condition has been proposed in [17][18].

3. DESCRIPTION OF THE TEST SETUP

GARTEUR AG24 shielding experiments are performed in the DLR Acoustic Wind tunnel in Braunschweig (AWB), as shown in Figure 2 for a sphere test with a sting support configuration. The AWB has a cross section of $(1.2 \times 0.8) m^2$. The open jet test section is known for its excellent flow quality and anechoic properties as well as its low background noise. For the sphere test, two sphere sizes, a small one with D1=0.12m diameter and a big one with D2=0.34m diameter are used. The sizes of the spheres are derived according to the largest dimension of the BO105 fuselage with 1/12.5 scale in lateral or streamwise directions. To quantify the influence of the sting support on the scattering results, the wire support (Figure 3), where the sphere is hanged with three 0.002m diameter wires, is also used. In addition, spheres of different materials (wood or aluminium) are also conducted.

The shielding setup for a 2D wing with NACA0012 profile is shown in Figure 4. The wing is mounted vertically in the test section with a dx=0.2 m shift away from the tunnel centerline. This is done to provide enough room for the inflow microphone (C) in Figure 4, to be placed in the geometric far-field of the model. The whole laser was tilted 3° towards the model, to avoid collision of the optical components with the wing's support when moving the source. A detailed description of the NACA0012 wing test can be found in [19].
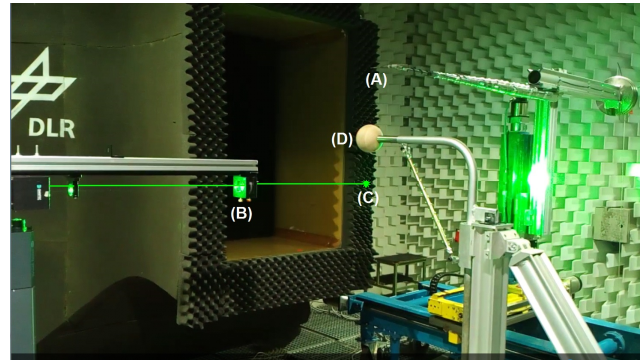
(a) Test set-up with laser point source
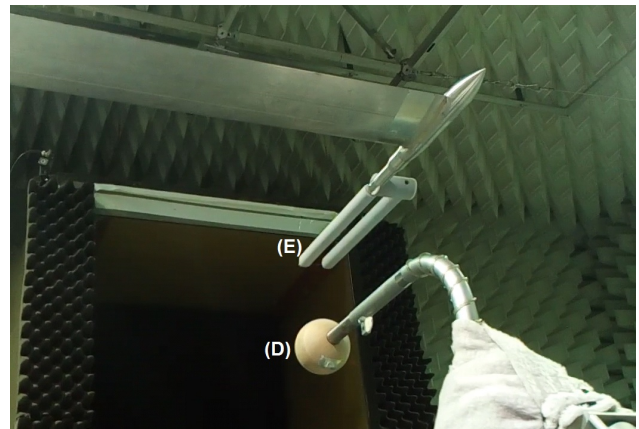
(b) Test setup with SPARC

Figure 2. Complete test set-up including either laser source (B,C) (a) or SPARC (E) (b), sphere with sting support (D) and microphone (A).
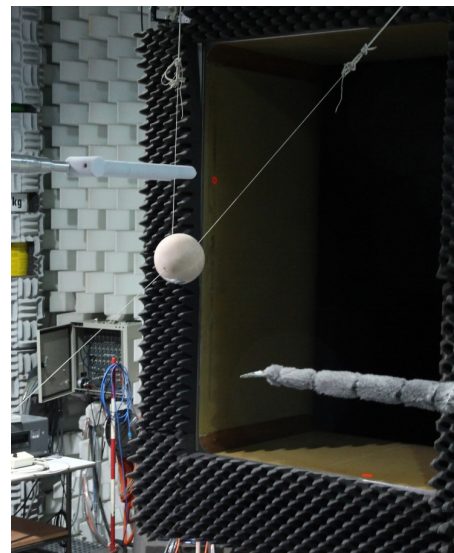

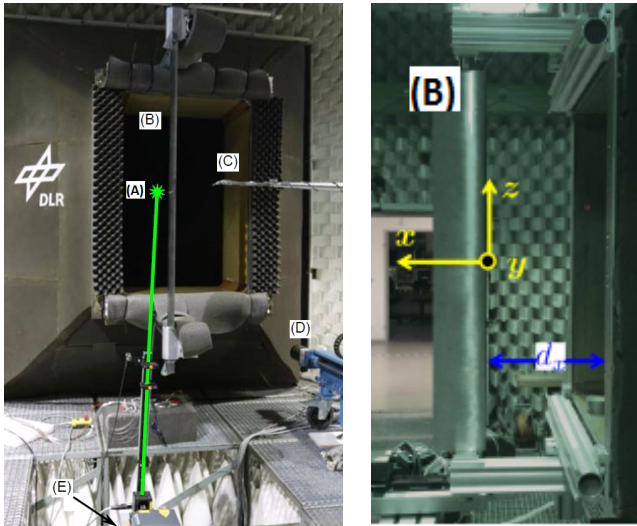**Figure 3. Sphere hanged by wires**

Figure 4. Shielding setup in AWB for 2D wing, Left: (A) Laser sound source, (B) NACA0012 2D wing, (C) microphone, (D) microphone positioning system, (E) laser sound source positioning system, Right: setup of the wing

3.1 Description of the noise sources

The choice of the noise sources is based on the criterion of non- or minimum-intrusiveness for both the mean flow and scattered acoustic field. As shown in Figure 2, two point-source systems are used. The first one is a laser plasma pulse system from DLR [20] as indicated as (C) in Figure 2a, and the other noise source is SPARC system of ONERA [21], as indicated as (E) in Figure 2b. Since the two sources have two different frequency ranges, they complement each other to provide a wider frequency domain.

3.1.1 DLR Laser Generated Sound

By focusing a high energy laser beam on a point, it is possible to initiate the formation of a small plasma which rapidly expands [22][23], thus forming a pressure wave about its boundary which propagates through the surrounding medium. The optical setup for the DLR laser sound source is shown in Figure 5, where the combination of one concave length and two convex lenses is applied to ensure plasma creation at about 500mm from last convex lens.
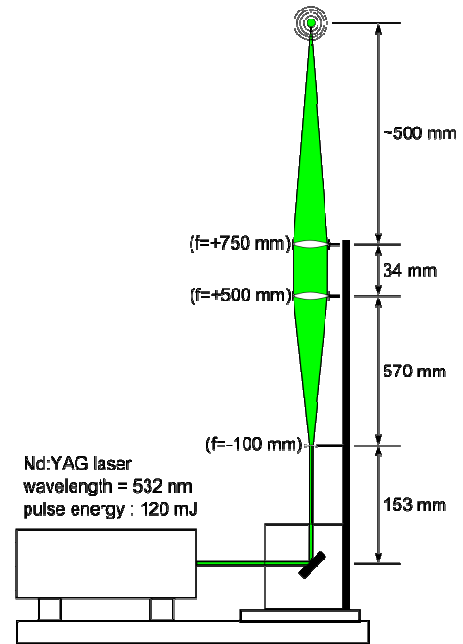
Figure 5. Optical setup for the laser sound source

The DLR laser sound source has the advantage of being non-intrusive for both mean flow and scattered acoustic field. Because of its small size and uniform directivity, it can be represented as a point monopole source.
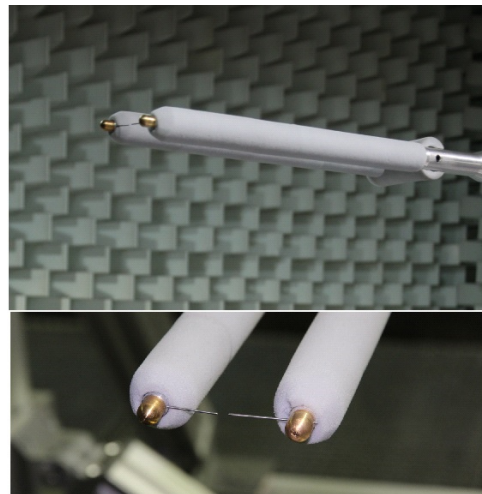

Figure 6. A detailed setup of the sharp probes from SPARC

### 3.1.2 ONERA SPARC (Source im Pulsionnelle AeRoaCoustique)

Above a given threshold, a strong electric field ionizes the air between two sharp probes [21]. In this way, an electrical channel is created and an abrupt current discharge occurs. A part of the released energy is then converted into heat in the small region between the probes. This intense heat induces a local expansion of the air which generates

an acoustic pressure wave. A detailed setup of the sharp probes is shown in Figure 6.

3.1.3   Acoustic Instrumentation
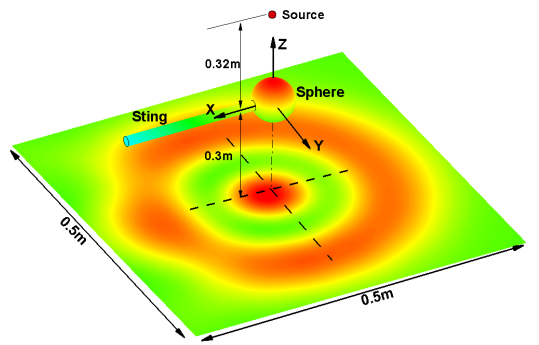
a) Axis system and traverse directions (dashed line)
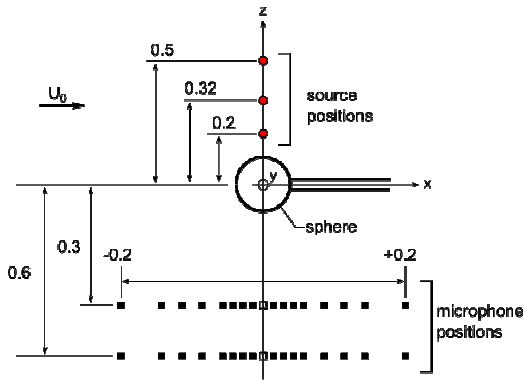
b) Source and microphone positions. Same microphone traverse for the y direction

Figure 7. The configuration with the sting support

In-flow measurements are performed using 1/8" inch Bruel & Kjäer pressure field microphones equipped with a standard nose cone. One microphone is installed at a fixed position near the ground and serves as a reference measurement.

The second microphone is mounted on a traversing system, which is either above or below the sphere, depending on the position of the source. The measurements were done on linear microphone traverses in both x direction aligned with the sting axis at y=0, and y direction at x=0, as shown in Figure 7.   As the spheres are located directly between the source and the microphone, the maximum sound shielding can be measured by the arrays. Two microphone traverses are necessary in order to test the influence of the support system, such as the sting. The coordinate center is chosen as the center of the sphere.

4.   RESULTS AND DISCUSSION

In the following sections, only a comparison of the shielding factor or attenuation factor γ_T from the tests or numerical results is conducted. The shielding factor is defined as the ratio of total pressure $p_{tot} = p_i + p_s$, and incident pressure p_i,

$$GT = \gamma_T(f) = \frac{p_{tot}(f)}{p_i(f)}$$

where p_s is the scattered acoustic pressure. The shielding factor deviation from value 1 can be considered as the effect of the scattering by the obstacles. When evaluating the shielding factor for the test result, the ensemble averaged total and incident pressure fluctuations are used to reduce the measurement errors. The advantage of using the shielding factor to evaluate the scattering effect is that no corrections on signal amplitude are required. In addition, when the microphone is equipped with a nose cone during the measurement, corrections on microphone directivity are not required.

4.1 Test results of sphere scattering for two noise sources

In this section, the test results of the sphere scattering by two different noise sources, DLR laser pulse and ONERA SPARC, are compared. The test results are also compared with the analytical solution, to verify the accuracy of the complete test system, such as support systems and noise sources, microphones as well as the reliability of the test results.

The measured shielding factors γ_T at f=3000Hz from the wood sphere hanged with wires (Figure 3) are shown in Figure 8 for the two different noise sources. The diameter of the sphere is 0.12m. The test results with DLR noise source using Laser fit well with the analytic solution (blue line) in both traversing directions, except for some deviations in the shadow region around x or y=0 m are noticed, where the microphones are located below the sphere. Similar observations are made for the ONERA SPARC source. The measured shielding factors from both noise sources capture the characteristics of the troughs and peaks of an interference pattern around the shadow region. The matching with the analytical results indicates that the wood sphere can be considered as acoustic hard sphere.
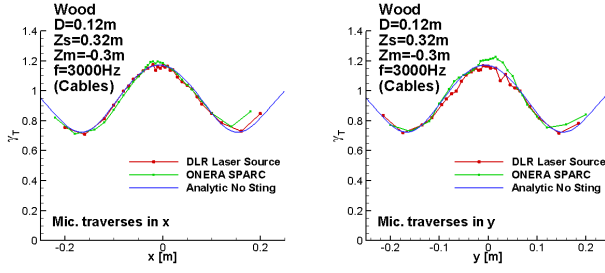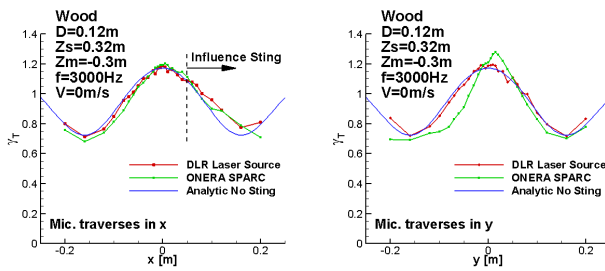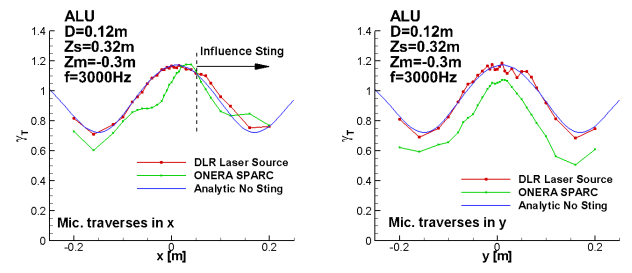
Figure 8. Measured shielding factor γ_T for the wood sphere D=0.12m with cable support at 3000Hz

Figure 9 (a) and (b) show the comparisons of measured shielding factor γ_T for both the aluminum and the wood sphere with the sting support (Figure 2). For the DLR laser source, the comparisons with the analytical results show that the general characteristics of the local peak and troughs from two types of spheres are well matching the analytical one. As the analytical solution was obtained for a solid surface without including the sting support, the deviations observed for x array in the positive x directions indicate the interference from the sting support. The deviations are similar for both spheres. The difference caused by the different material cannot be identified since the results are almost independent of the materials. For the ONERA SPARC source, the comparisons with both the analytical results and DLR results indicate large deviation for the aluminum sphere, especially for y-traversing where a clear offset is observed. For the wood sphere, the deviation caused by the sting support fitted well with the results from DLR source. There are several possible reasons that might contribute to the difference. The possible reasons are the interferences of source probes on the sound propagation, disruption of the metal sphere on ionized electric field, and relative lower signal to noise ratio at 3000Hz.
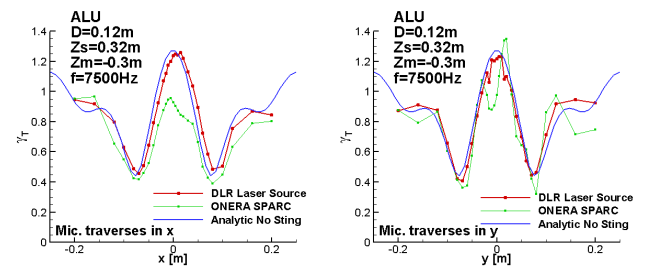

(a) Measured shielding factor for the wood sphere, Left: X-traverse, Right: Y-traverse
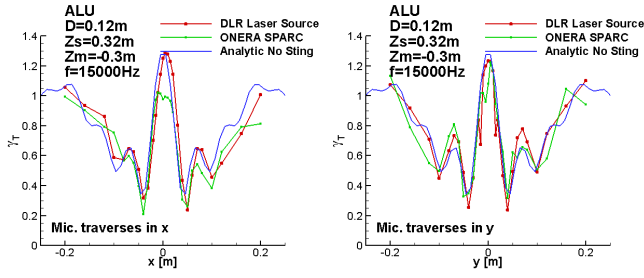
(b) Measured shielding factor for the aluminum sphere, Left: X-traverse, Right: Y-traverse

Figure 9. Shielding factor γ_T for the aluminum (a) and the wood sphere (b), Diameter D=0.12m, with sting support at 3000Hz

Figure 10 (a) and (b) show the comparisons of the measured shielding factor γ_T for the aluminum sphere at higher frequencies of 7500 and 15000Hz. As the acoustic signal at 7500Hz or above has a wave length smaller than the characteristic length of the small sphere diameter D1=0.12m, the interference pattern in space, as shown in Figure 10, indicates an increasing number of side lobes in the shadow area when increasing the frequency. The width of both the side lobes area and peaks becomes narrower when increasing the frequency. In general, the test results using both DLR laser source and ONERA SPARC have captured all the characteristics of the interference pattern in space, except large deviation occurring in the shadow region around x or y=0 m for ONERA SPARC, which may be caused by disruption of metal sphere on ionized electric field as mentioned before. In addition, good correlation for ONERA source for these two frequencies indicates higher signal to noise ratio in the high frequency range. As the acoustic signal at 15000Hz has a wave length close to the diameter of the sting (D=0.028m), a relative large influences of the sting support for the shielding factor are expected for microphones beneath the sting (positive x).

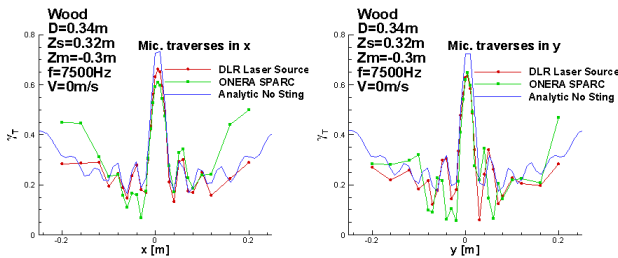(a) Measured shielding factor at 7500Hz, Left: X-traverse, Right: Y-traverse

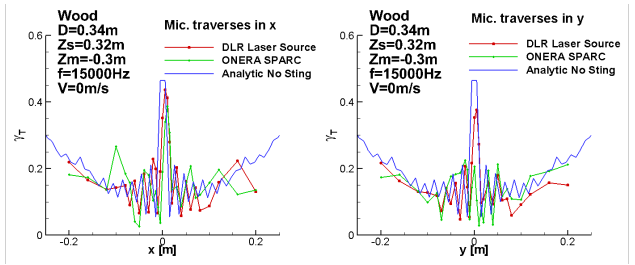(b) Measured shielding factor at 15000Hz,
Left: X-traverse, Right: Y-traverse

Figure 10. Shielding factor for the aluminum sphere D=0.12m with sting support at 7500 and 15000Hz

The measured shielding factors for the large wood sphere (D=0.34m) at f=7500Hz and 1500Hz are given in Figure 11. For the large sphere the interference patterns become more complicated, showing more side lobes. The shielding factors exhibit a narrow shadow region and lower value of the shielding factor in comparison with the small sphere for this frequency. For the large sphere, strong reflections of the acoustic energy at the sphere surfaces causes a large shadow region (<<1) in all measurement area. The experimental results for two noise sources at 7500Hz show a behavior similar to the analytic solution without sting and therefore demonstrate the small effect of the sting. In addition, the test has captured at least the first two side lobes. For noise source at f=15000Hz, the test results using DLR source still demonstrate satisfactory comparison in terms of the troughs and peaks of an interference pattern around the shadow region, while ONERA SPARC misses the main interference peak directly underneath the sphere for the y traversing.

In general, for the considered frequency range, notwithstanding some level of disagreement in representing the side lobes, the experimental results are comparable with the analytical ones with acceptable accuracy.
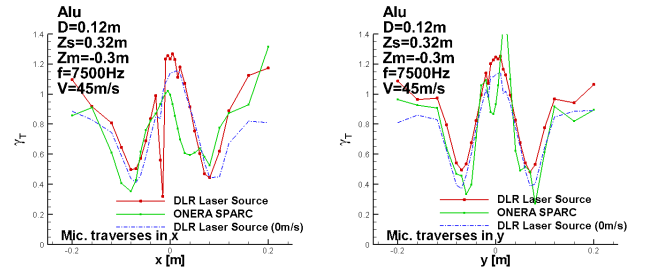

(a) Measured shielding factor at 7500Hz,
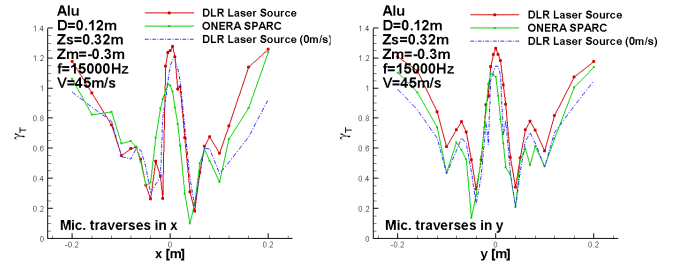Left: X-traverse, Right: Y-traverse

(b) Measured shielding factor at 15000Hz,
Left: X-traverse, Right: Y-traverse

Figure 11. Shielding factor for the wood sphere D=0.34m with sting support at 7500Hz

Figure 12 shows the comparisons of the shielding factor in the condition of presence of a mean flow (V=45m/s) at two frequencies. For comparison, the test results from DLR laser source at V=0 m/s are also included.

(a) Measured shielding factor at 7500Hz,
Left: X-traverse, Right: Y-traverse

(b) Measured shielding factor at 15000Hz,
Left: X-traverse, Right: Y-traverse

Figure 12. Effect of the mean flow with 45m/s on shielding factor for the sphere D1=0.12m with sting support

Direct comparisons of the results from two noise sources indicate that, with the exception of the large deviation occurring in the shadow region around x or y=0 m, both sources demonstrate the same trends for upstream and downstream traverses in x direction as well as in lateral direction in y. The DLR source shows a sharp drop in shielding factor occurs in the upstream part of the x-traversing, just before the main peak: the reason of this drop still needs to

be further investigated. The effect of the presence of the mean flow is in general to increase the level of the shielding factor for both array traverse directions. For x traversing, the shielding factor increases quickly with increasing downstream distance.

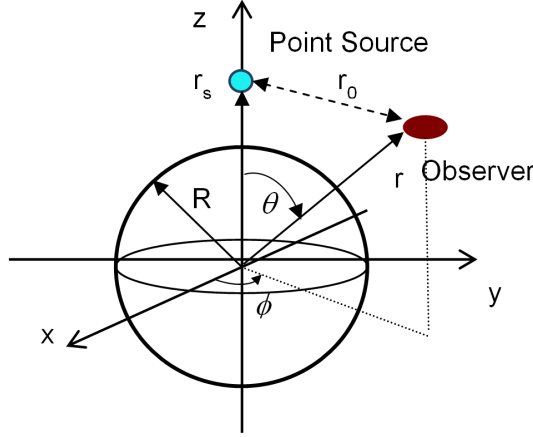## 4.2 Numerical simulation results

4.2.1 Scattering from sphere

Figure 13. Scheme of acoustic scattering of a point monopole source by a sphere

One of the main objectives of the GARTEUR AG24 is the assessment through validation of the acoustic scattering prediction capabilities available within the group and the possible improvement of the existing tools. The numerical simulations were first conducted for the sphere scattering from a point source with two sphere sizes (D1=0.12m and D2=0.34m), and various source positions and frequencies. The simulations were first validated with the analytical solution. The schematic relation of the source and observer or microphone in these first simulations is given in Figure 13.

The effect of the geometry discretization can be classified representing the grid size in terms of Points Per Wavelength (PPW). The code-to-code comparisons were conducted using, when possible, the same number of PPW. The grid size ΔX can be defined according to a given PPW; for example for a given PPW, the actual size ΔX of the grid cells is:

$$\Delta X(m) = 340(\frac{m}{s})/f(Hz)/PPW$$

| PPW	F=2500(Hz)	5000(Hz)	7500(Hz)
7	ΔX=0.01943m	0.00971m	0.00648m
14	0.00971m	0.00486m	0.00324m
28	0.00486m	0.00243m	0.00162m

**Table 1. grid size ΔX as function of frequency and PPW**

The large values of PPW correspond to a fine surface grid and therefore lead to large computation times. Three different PPW values were chosen in the comparison, as given in Table 1.

The comparison of the simulated shielding factor γ_T has been plotted in

Figure 14 for the small sphere of the diameter D1=0.12m in a polar directivity plot at three frequencies. Results refer to a point source placed at r_s=0.32m from the center of the sphere; the sphere surface is discretized with PPW=14 and the shielding factor were taken from a r=0.6m circle as shown in Figure 13. All methods give similar trends which are in good agreement with analytical results. This is especially true when considering the BEM results, which are very close and collapse on the analytical solution. As expected, somewhat poorer results are provided by the flat approximation method of the KIM code. Results obtained with the latter method are improved at high frequency but the area between approximately 120° and 240° (shadow zone) is always of poor accuracy. The method only predicts reflection (by supposing a surface locally flat) and ignores refraction. Consequently, the sphere test case is particularly unadapted for this approach. However, the rapidity of this approach has to be taken into account when looking at the accuracy.
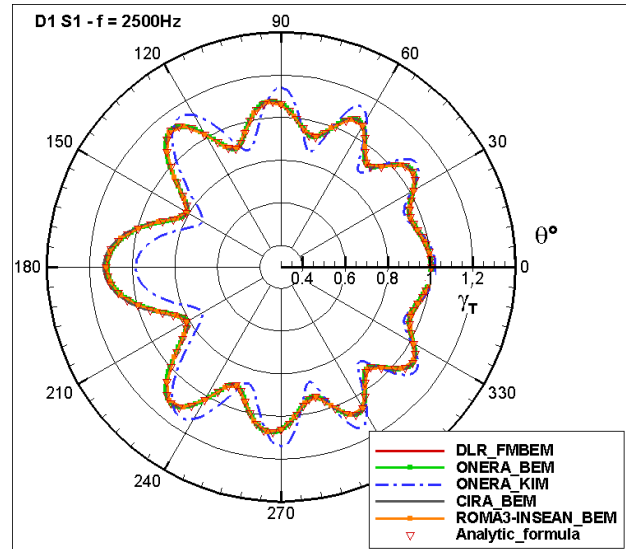
f=2500Hz
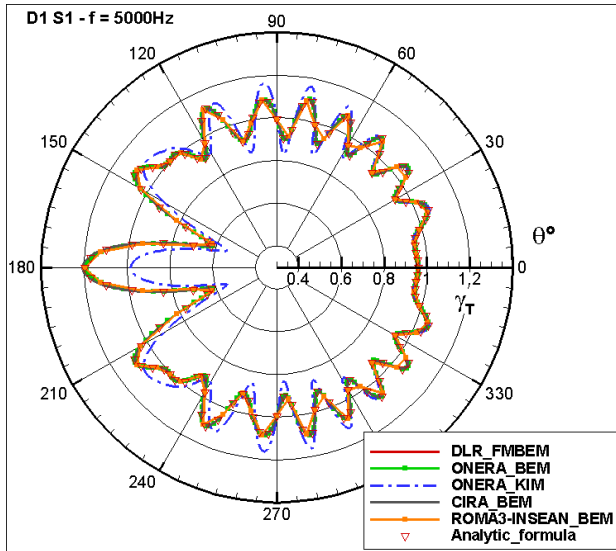
f=5000Hz
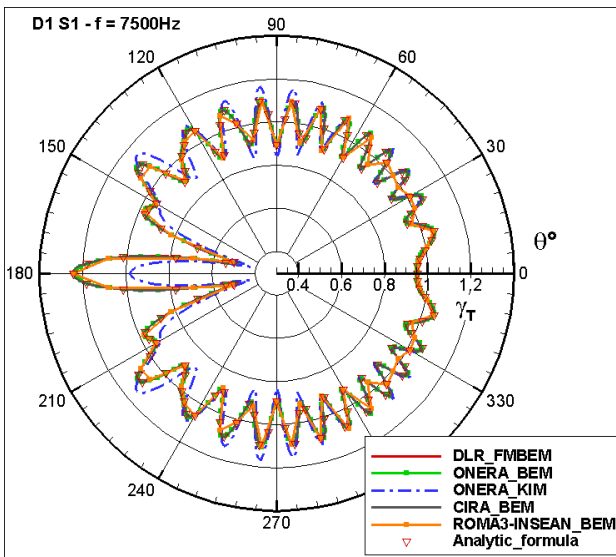
f=7500Hz

Figure 14. Comparison of the scattering directivity from the sphere D1=0.12m and source S=0.32m, at three different frequencies. PPW=14

For the large sphere ($D2 = 0.34m$), the scattering at 2500Hz is shown in Figure 15, where NLR CAA results are also included. The shielding factors exhibit a narrow shadow region and lower value of the shielding factor in comparison with the small sphere for this frequency as shown in
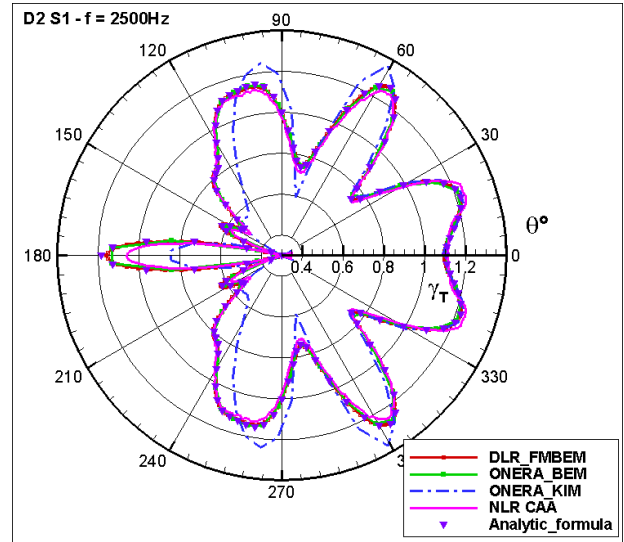
Figure 14.

Figure 15. Comparison of the scattering directivity from the sphere D2=0.34m and source S=0.32m, f=2500Hz. PPW=14

All BEM methods show a good agreement with analytical results. The CAA results from NLR show some amplitude error near the 180° angle. Such behaviour may be caused by the applied monopole source model, which smoothly distributes the forcing over a few cells. Therefore, it does not capture exactly the singular behavior of the monopole. For NLR CAA method, a grid refinement level of 14PPW is required to reduce the impact of artificial damping that was introduced to counteract spurious modes.
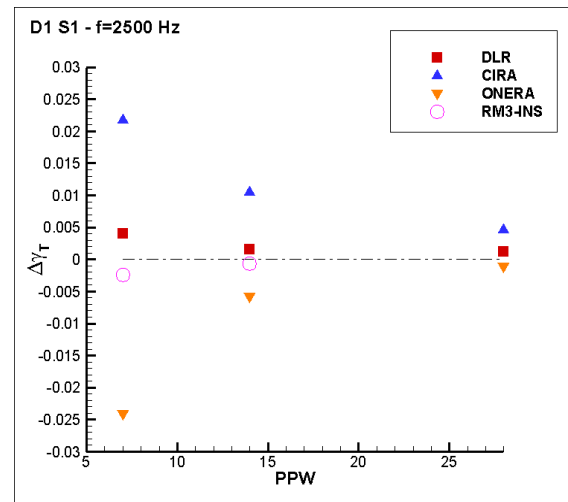

Figure 16. Influences of the numerical discretization error at 2500Hz

The influences of the numerical discretization in terms of PPW at 2500Hz are summarized in Figure 16. The results indicate absolute errors with respect to the analytic solution, taken from a point in the shadow region at θ=180°, where the microphones are located direct below sphere and opposite to the

source. In this position, the largest interferences between direct and scattered wave occur.

The convergence results with all BEM methods are very similar. The study highlights the general high level of accuracy of the acoustic scattering models in capturing the analytical solution in terms of magnitude and directivity.

4.2.2 Scattering from Sphere + Sting

The numerical simulations for the configuration with the sting support, as shown in Figure 7 are conducted in order to demonstrate the influence of the sting and to compare with test results. Only the horizontal part of the sting with a length 0.3867m and diameter (D=0.028m) is represented, but not the sting support system as show in Figure 2. In order to avoid discrepancies in the scattering results, the chosen mesh is critical for all simulation methods. Therefore a common surface grid is used. The average grid resolution is 0.00324m which corresponds to 14 PPW at 7500Hz. The size of the computation domain, source and microphone positions is shown in Figure 7. A point source is located at 0.32m on the z axis above the sphere and the size of the sphere chosen for this example is D1=0.12m. Two dashed lines represent the two traverse directions used in the measurements.

Figure 17 shows the contour plot of the shielding factor on a receiving plane (microphones) given in Figure 7 for two different frequencies, 3000Hz and 7500Hz. The general shielding characteristics can be observed by the shielding pattern composed by the higher and lower levels in the plot. The higher and lower levels are represented by different colors. The "silent zone" directly below the sphere, where no incident wave can be propagated, is determined entirely by the diffracted waves, which has a small peak showing in red areas. Due to the contribution of the diffraction waves from the sting support, the shielding pattern is no longer symmetric, especially for the area underneath the sting in positive x direction. In general, the complexity of the scattering pattern increases with increasing frequency. An increase of higher and lower shielding bands in upstream direction of the sphere (negative x direction) is observed with increasing frequency. As for the isolated sphere, the FSA approach proposed by ONERA provides a good qualitative prediction. The comparison of the values taken directly from the microphone traverse (marked as dashed line in Figure 7) is given in Figure 18 together with the experiment results.
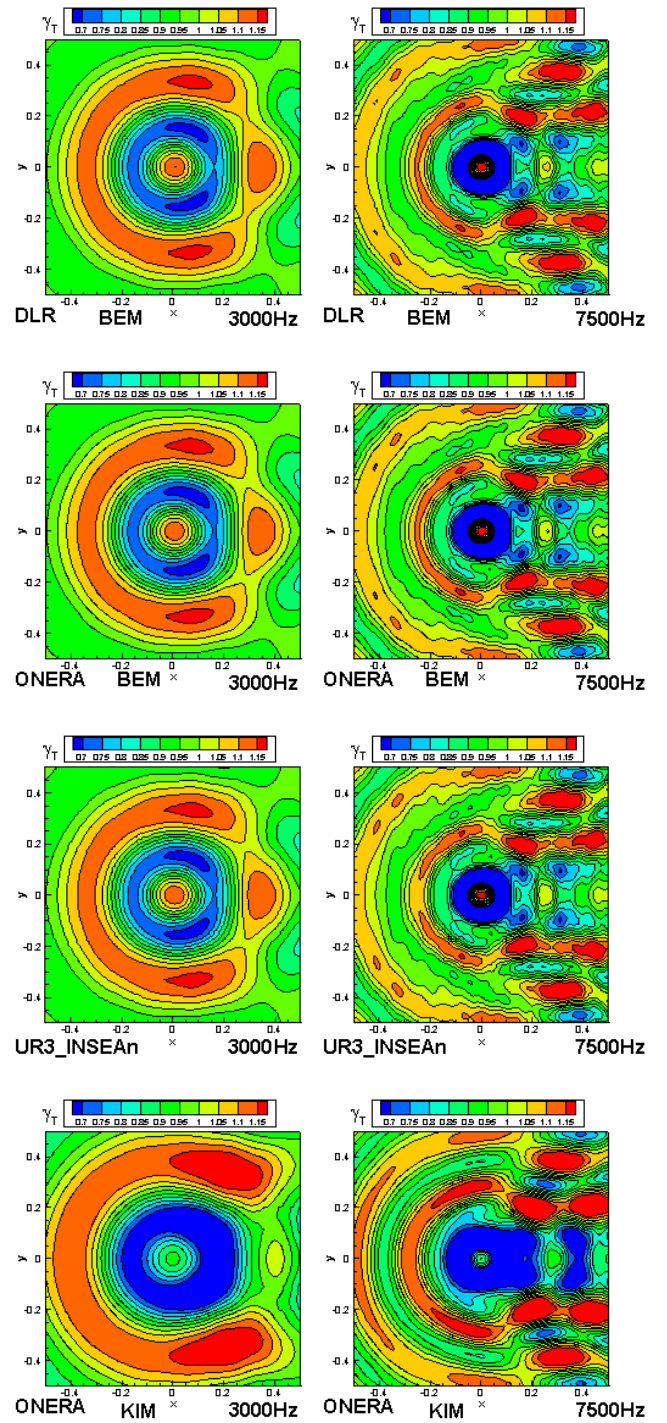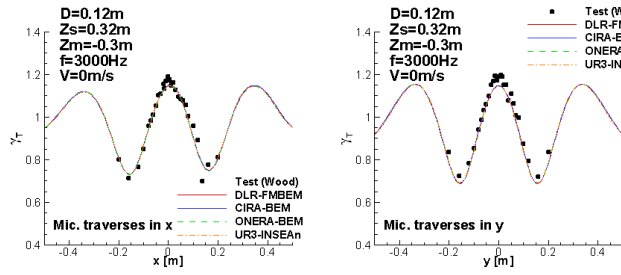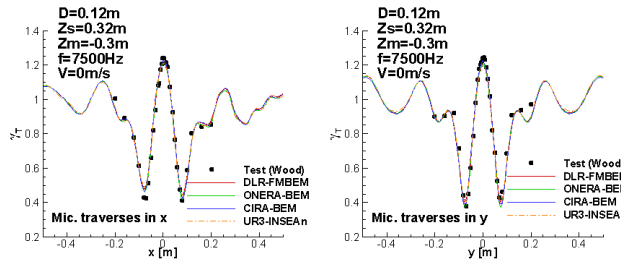

Figure 17. Contour plot of shield factor for the sphere+sting D=0.12m at f=3000Hz,7500Hz, with V0=0 m/s

(a) shielding factor at 3000Hz,
Left: X-traverse, Right: Y-traverse

(a) shielding factor at 7500Hz,
Left: X-traverse, Right: Y-traverse

Figure 18. Comparison of the shielding factor with test for the sphere D1=0.12m with sting support

The comparisons of the shielding factor with the experimental data show very good correlations in terms of amplitude and phase. The asymmetry of the scattering in x-direction under the influence of sting is captured by all participants.

Figure 19 shows the contour plot of the shielding factor under influence of mean flow (V=45m/s) at 7500Hz. Compared to Figure 17 (right, BEM results of both DLR and ONERA), the shielding factor with mean flow shows quite similar pattern because the uniform flow assumption in the simulations does not change the way the acoustic waves are scattered. The comparison with the experimental data, taken directly from the traverse microphone in Figure 20 shows a reasonable agreement with numerical simulations. The agreement between ONERA and DLR BEM results is excellent in both traverse directions.
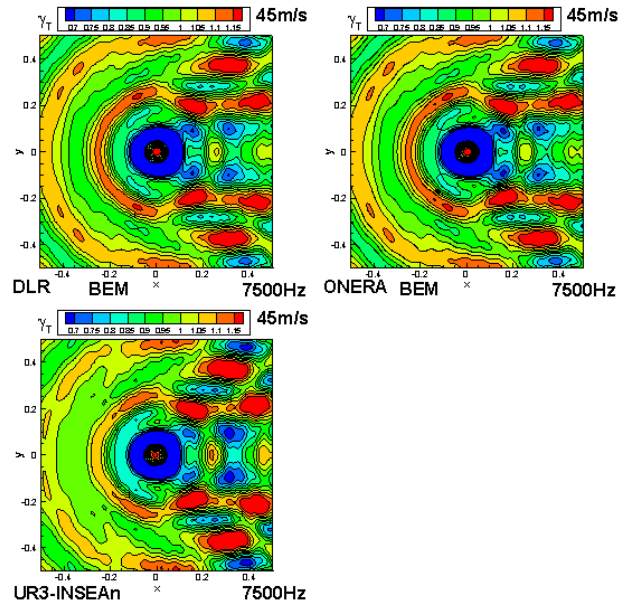

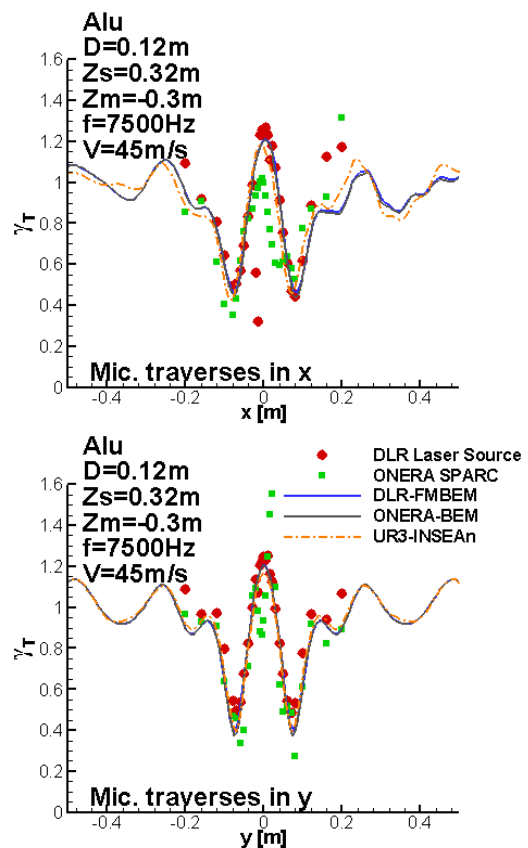**Figure 19. Contour plot of shield factor for the sphere D1=0.12m at f=7500Hz with V0= 45m/s**

Figure 20. The comparison of the shielding factor with test for the sphere D1=0.12m with mean flow 45m/s, Top: X-traverse, Bottom: Y-traverse

4.2.3 Scattering from NACA 0012 wing

For a further assessment of the acoustic scattering prediction capabilities, the test cases conducted in the NATO STO (AVT 233 RTG-078) Group have been chosen for the predictions [19]. The experimental data are provided by STO group for the validation. The wind tunnel setup, the coordinate system as well as relative position between source position (solid red circles) and microphones (black open circle) is shown in both Figure 4 and Figure 21. The microphones are located in the symmetry plane. The selected results from source position S1 (-0.05,0.0,-0.025) and S3 (0.05,0.0,-0.036841), as indicated in Figure 21 top, will be compared and flow effect will be discussed. The airfoil chord length is C=0.2m. The comparison will be made on the microphone array position, also shown with the red line in Figure 21 bottom.
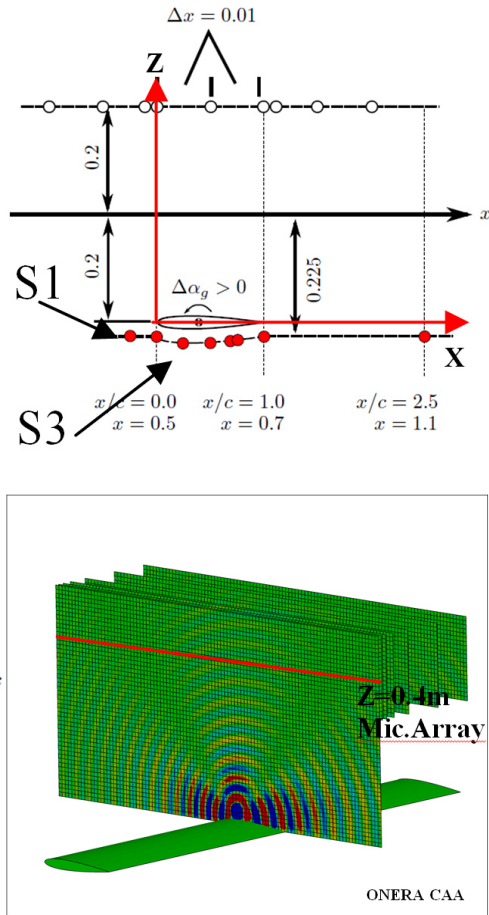

Figure 21. Wind tunnel setup, coordinate system as well as relative position between source position (solid red circles) and microphones (black open circle) for the NACA 0012 test
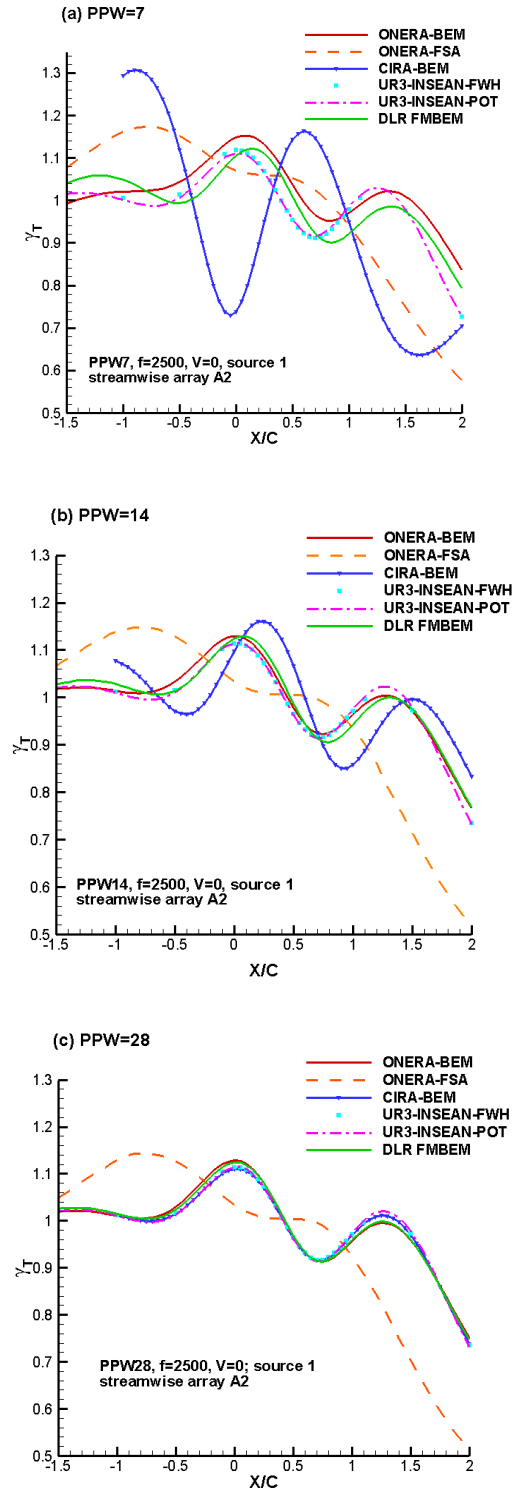

Figure 22. Shielding factor as function of PPW, Source at S1; f=2500Hz; V=0.0m/s

The Effect of the discretization is first studied by varying PPW. All partners use identical meshes with the exception of the University of Roma using structured grids. Figure 22 shows the shielding factor as function of PPW for noise source located at S1 with zero flow. The scatter of the results at lower

PPW indicates that the results are more sensitive to the PPW compared to the sphere case. 7 PPW is not enough to discretize the leading edge of the wing. Almost all BEM formulations tend to coincide with increasing spatial resolution to PPW 28, as can be observed in Figure 22 (c). The FSA formulation gives good tendencies even if results are different from the BEM formulations. It has to be pointed out that FSA method is much simpler and faster than traditional BEM and only reflections are considered, therefore FSA should not be considered at the same level of modeling.

A detailed study on the effect of the discretization was conducted by CIRA. Three different meshes were analyzed by refining the mesh near the LE and closing the tip surfaces. The computation performed by CIRA, not shown here, demonstrated that the NACA0012 scattering solution is very sensitive to the mesh used especially for discretization of the leading edge.

The comparison of the numerical simulations with the experiment results for source position S3 (Figure 21) is given in Figure 23 for two frequencies. All methods give similar trends and good correlation with the experiment results. Different from the source at S1, the simulation results are not coincide even with the high spatial resolution PPW 28. The large deviations among the simulations occur for the microphone positions above the leading edge (x=0) for f=2500Hz, while for 5000Hz the deviations spread to almost all microphones and especially for far negative x. The deviations among the simulations indicate different refinement of the mesh near the LE as well as matter of different grid resolutions used by partners, due to limitation of different code capabilities.
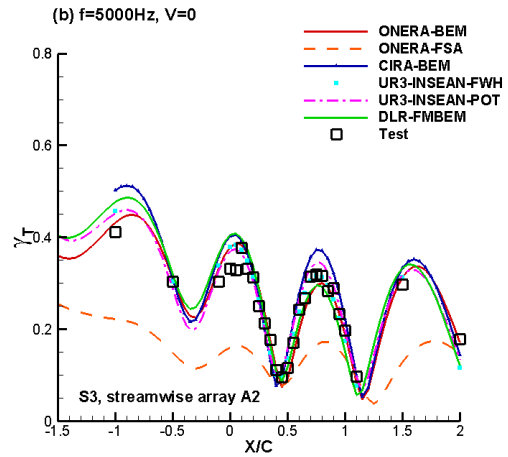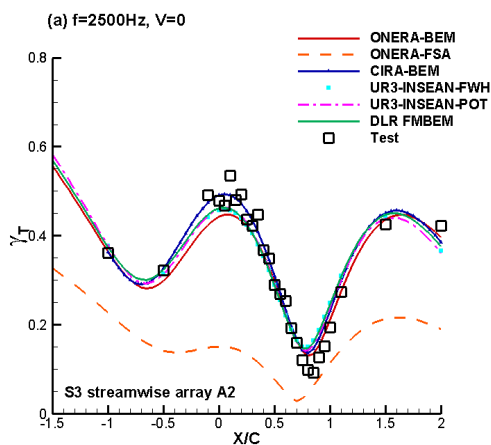

(a) f=2500Hz, V=0

Figure 23. Comparison of measured and simulated shield factor for Source S3 without mean flow V=0m/s, PPW=28

Figure 24 shows the comparison of the shielding factor for source position S3 with mean flow speed V=55m/s for two frequencies. All calculations assume uniform flow, except ONERA with potential flow. The results with mean flow have similar characteristics as the results without mean flow as shown in Figure 23, indicating minor influence of the flow on the shielding factor. As DLR and ONERA method take into account flow effect using the Taylor transformation as described in [13], the same correction is applied on the incident field and the total field. Therefore there is very little flow effect when looking at the shielding factor.

In this case higher discrepancies appear. These are due to the effects deriving from the different approximations the applied formulations are based on. For instance, those based on Taylor Transform neglect M_∞^2 terms affecting both surface integral contribution and acoustic delay. The Taylor transformation is clearly an approximation but when looking at the comparisons with CAA in Figure 25 the result is satisfactory for a uniform flow.

It is interesting to observe that in addition to the free-stream Mach number, the scatter geometry strongly affects the amplitude of the discrepancies between the results given by different models (see for instance Figure 18 as compared with Figure 24). Even with same methodology used by DLR and ONERA, there are still some discrepancies especially for the higher frequency (5000Hz) in the area X/C<0. The discrepancies may be caused by different discretization of the leading edge and there are still needs further studies.
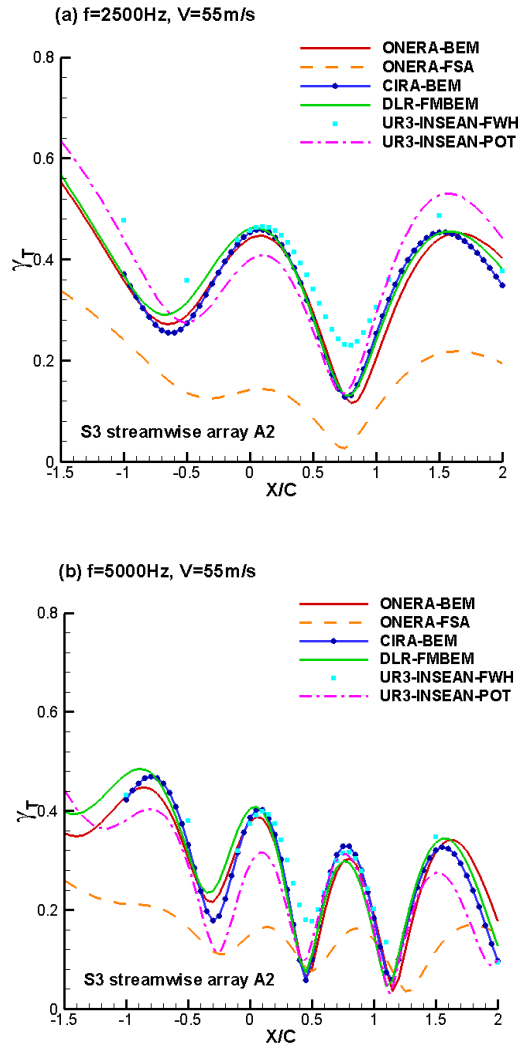
(a) f=2500Hz, V=55m/s

S3 streamwise array A2

(b) f=5000Hz, V=55m/s

S3 streamwise array A2

Figure 24. Simulated shield factor for Source S3 with mean flow V=55m/s, PPW=28

Further analyzes are proposed in Figure 25. BEM and FSA results are compared to CAA simulation performed by the ONERA sAbrinA solver which has the capacity to properly take into account non-uniform mean flow. It is important to notice that the comparison is made closer to the airfoil at Z=0.1m to reduce CAA computational time. First of all, in Figure 25a), the comparison is performed without flow. A very good agreement is obtained when comparing BEM and CAA results. Once again, the FSA results are of poorer accuracy but capturing the general trends. In Figure 25b), flow effects are taken into account. When only a uniform flow is taken into account, the impact is weak for all methods involved and the agreement between BEM results are still accurate compared to CAA results. It is also noticeable that the ONERA BEM simulation taking into account potential flow reacts actually just like a uniform flow case. On the other hand, when a

potential non-uniform flow is considered, CAA results appear to be impacted especially in the upstream direction. This is again explained by the fact that the uniform flow does not change the way the acoustic waves are scattered. The effect is the same on both direct, incident and scattered wave. This is not the case when non-uniformity of the flow is encountered by acoustic waves in the vicinity of the airfoil.
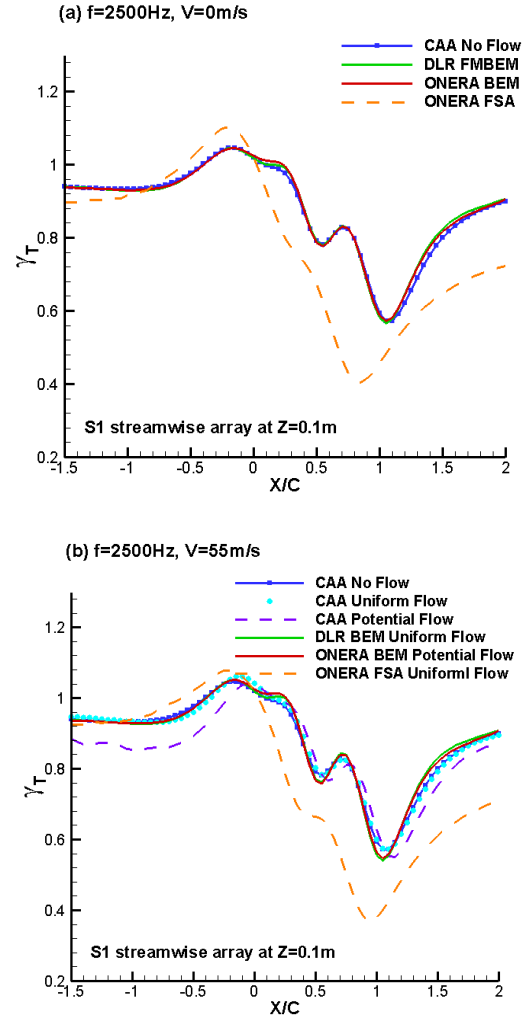

(a) f=2500Hz, V=0m/s

S1 streamwise array at Z=0.1m

(b) f=2500Hz, V=55m/s

S1 streamwise array at Z=0.1m

Figure 25. Comparison with ONERA CAA, for Source S1 with mean flow V=55m/s, PPW=28

CONCLUSIONS

In this paper, experimental and numerical investigations of the shielding characteristics of both sphere and wing are presented. Comparisons of code-to-code and the code-to-test results or code-to-analytical solutions were carried out. The configurations, herein investigated, are the rigid nonmoving spheres and wing impinged by the sound waves emitted by a monopole. The test results are derived from noise source generated from either

DLR laser pulse or ONERA SPARC. The numerical comparisons were conducted among different solvers available within the Action Group AG24.

Following concluding remarks can be drawn:

Test results from both DLR laser-based and ONERA SPARC noise source capture the general characteristics of the noise shielding effect from a point monopole. The noise shielding results using DLR laser-based non-intrusive sound source provide clear and consistent trends for all considered cases. The results from ONERA SPARC however indicate large deviation for the aluminum sphere. The possible reasons are the interference of source probes on the sound propagation and the disruption of metal sphere on ionized electric field.

The numerical simulation results for sphere scattering indicate that the BEM methods achieve high level of accuracy of the acoustic scattering models in compared to the analytical solution. The spatial convergence results with all BEM methods are very similar. The shielding factor with mean flow shows quite similar pattern as the one without flow. This is also true for the numerical predictions, although the uniform flow assumption in the simulations does not change the way the acoustic waves are scattered.

The assessments of the acoustic scattering from the NACA0012 wing indicate the scattering solution is very sensitive to the mesh used, especially to the discretization of the leading edge. Again BEM methods give similar trends and good correlation with the experiment results. The results with mean flow resemble same characteristics as the results without mean flow.

ACKNOWLEDGMENTS

COPYRIGHT STATEMENT

REFERENCES

[1]. J. Yin, M. Barbarino, H. Brouwer, G. Reboul, M. Gennaretti, G. Bernardini, C. Testa, L. Vigevano, "Helicopter Fuselage Scattering Effects for Exterior/Interior Noise Reduction", Terms of Reference for the GARTEUR Action Group HC/AG-24, April 2015.

[2]. M. Barbarino, D. Bianco, J. Yin, M. Lummer, G. Reboul, M. Gennaretti, G. Bernardini, C. Testa, "Acoustical methods towards accurate prediction of rotorcraft fuselage scattering", 42nd European Rotorcraft Forum, September 5-8, Lille, France, Paper 62, 2016

[3]. [3]. J. Yin, K-S. Rossignol, J. Bulté, "Acoustic scattering experiments on spheres for studying helicopter noise scattering", 42nd European Rotorcraft Forum, September 5-8, Lille, France, Paper 127, 2016

[4]. M. Barbarino, "Aeroacoustic Methods for Low-Noise Technologies Design", PhD Thesis, Federico II University, Naples, 2013.

[5]. M. Barbarino, D. Bianco, "BEM-FMM simulation of uniform mean flows with a new internal-point algorithm for the CHIEF spurious solutions removal", Proceedings of the 23rd International Congress on Sound & Vibration, 10-14 July, 2016.

[6]. M. Lummer, C. Richtery, C. Pröber, J. Delfs, "Validation of a Model for Open Rotor Noise Predictions and Calculation of Shielding Effects using a Fast BEM", 19th AIAA/CEAS Aeroacoustics Conference (34th AIAA Aeroacoustics Conference), 27 - 29 May 2013.

[7]. J. C. Kok, "Computation of sound radiation from cylindrical ducts with jets using a high-order finite-volume method", 13rd AIAA/CEAS Aeroacoustics Conference, AIAA paper 2007-3489 (NLR-TP-2007-514), Rome, Italy, 21 - 23 May 2007.

[8]. G. Rahier, and J. Prieur, "An efficient Kirchhoff integration method for rotor noise prediction starting indifferently from subsonically or supersonically rotating meshes", AHS forum 53, Virginia Beach, May 1997.

[9]. Juvigny, X., "A Fast algebraic boundary integral solver", 8th World Congress on Computational Mechanics, Venise, Italy, June 2008.

[10]. V. Rokhlin, "Rapid Solution of Integral Equations of Classical Potential Theory", Journal of Computational Physics, 60, 187–207, 1985.

[11]. A. J. Burton, G. F. Miller, "The Application of Integral Equation Methods to the Numerical Solution of Some Exterior Boundary-Value

Problems", Proc. R. Soc. Lond. A 1971 323 201-210; DOI: 10.1098/rspa.1971.0097. Published 8 June 1971.

[12].   L. Grasedyck, "Adaptive Recompression of H-matrix for BEM". Technical Report 17, Max-Planck- Institut fur Mathematik in den Naturwissenschaften, Leipzig, 2004.

[13].   Agarwal and Dowling, "The Calculation of Acoustic Shielding of Engine Noise by the Silent Aircraft Airframe", 11th AIAA/CEAS Aeroacoustics Conference, AIAA 2005-2996, 2005

[14].   S. Redonnet, E. Manoha and P. Sagaut, "Numerical Simulations of Propagation of Small Perturbations Interacting with Flows and Solid Bodies", Proceedings of 7th AIAA/CEAS Aeroacoustics Conference, May 2001.

[15].   D. C. Mincu, T. Le Garrec, S. Péron and M. Terracol, "Immersed boundary conditions for high order CAA solvers - Aeroacoustics installation effects assessment", 23rd AIAA/CEAS Aeroacoustics Conference, 5-9 June 2017, Denver, Colorado.

[16].   M. Gennaretti, C. Testa, "A Boundary Integral Formulation for Sound Scattered by Elastic Moving Bodies". JSV-D-06-00750, JOURNAL OF SOUND AND VIBRATIONS, 2008.

[17].   M. Gennaretti, G. Bernardini, C. Poggi, C. Testa, "A Boundary-Field Integral Formulation for Sound Scattering of Moving Bodies", AIAA-2016-2715 – 22nd AIAA/CEAS Aeroacoustics Conference Lyon (Fr), June 2016.

[18].   M. Gennaretti, G. Bernardini, C. Poggi, C. Testa, "Lighthill Equation-based Boundary Integral Formulations for Sound Scattering of Moving Bodies", AIAA-2017-3514 – 23nd AIAA/CEAS Aeroacoustics Conference Denver (USA), June 2017.

[19].   K.-S. Rossignol, J. Delfs. "Analysis of the Noise Shielding Characteristics of a NACA0012 2D Wing", 22nd AIAA/CEAS Aeroacoustics Conference, Lyon, France, 2016

[20].   K.-S. Rossignol, J. Delfs, F. Boden, "On the Relevance of Convection Effects for a Laser-Generated Sound Source", 21th AIAA/CEAS aeroacoustics conference, AIAA 2015-3146 Dallas, USA, June 2015

[21].   P. Lebigot, J. Bulté, R. Davy, F. Desmerger, L. Coste, "SPARC: Source imPusionnelle AéRoACoustique", ONERA Technical Report (in French), N°4/22699, 2015.

[22].   N. Hosoya, M. Nagata, I. Kajiwara, "Acoustic testing in a very small space based on a point sound source generated by laser-induced breakdown: Stabilization of plasma formation", Journal of Sound and Vibration, Vol. 332, No. 19, 2013, pp. 4572-4583

[23].   L. Radziemski, D. Cremers, "Laser induced plasmas and applications", Marcel Dekker Inc., New-York, June 1989